IEEE Access
Multidisciplinary ⋮ Rapid Review ⋮ Open Access Journal

Received 27 December 2023, accepted 12 January 2024, date of publication 16 January 2024, date of current version 5 February 2024.

Digital Object Identifier 10.1109/ACCESS.2024.3354773

RESEARCH ARTICLE

Modeling of the Gate Bias-Dependent Velocity–Field Relationship and Physics-Based Current-Voltage Characteristics in AlGaN/GaN HFETs

MINGYAN WANG[1], YUANJIE LV[2], HENG ZHOU[1], PENG CUI[3], AND ZHAOJUN LIN[1]

[1]School of Integrated Circuits, Shandong University, Jinan 250100, China
[2]National Key Laboratory of Application Specific Integrated Circuit, Hebei Semiconductor Research Institute, Shijiazhuang 050051, China
[3]Institute of Novel Semiconductors, Shandong University, Jinan 250100, China

Corresponding author: Zhaojun Lin (linzj@sdu.edu.cn)

This work was supported by the National Natural Science Foundation of China under Grant 11974210.

ABSTRACT In this paper, a gate bias-dependent velocity-field relationship model and a physics-based analytical model of current-voltage characteristics in AlGaN/GaN HFETs are developed. Based on Monte Carlo simulations, the experimental phenomenon that the channel electron velocity varies with the gate voltage is successfully reproduced. A modified gate bias-dependent velocity-field relationship model is established to obtain the velocity-field relationship of our fabricated AlGaN/GaN HFETs considering Polarization Coulomb Field (PCF) Scattering. This new velocity-field model can accurately describe the experimental phenomenon of velocity modulation by various gate biases and effectively reduce the fitting parameters. The parameters of the velocity-field model are incorporated into the compact model. The method cleverly maintains the direct relation between the velocity-field model parameters and AlGaN/GaN HFETs. All parameters have a specific physical meaning in our compact model and parasitic resistance factors and channel modulation effects are also incorporated. We validate the model with experimental data for AlGaN/GaN HFETs with gate lengths of 0.2 μm and 0.35 μm, respectively, and obtain good agreement.

INDEX TERMS Monte Carlo, compact model, velocity-field relationship, AlGaN/GaN HFETs, polarization Coulomb field scattering.

I. INTRODUCTION

With the development of AlGaN/GaN HFET processes and circuits, several compact models [1], [2], [3] have been developed to characterize and optimize AlGaN/GaN HFET device performance. An accurate velocity-field model and related Monte Carlo (MC) data are essential to creating a current-voltage (I-V) model. A peak electron velocity of 1.4×10^5 m/s was obtained based on the S-parameter measurements by Romanczyk et al. [4]. As the negative gate bias increases, the channel electron velocity decreases [4]. Based on a time-delay method, Leach et al. reported the experimental phenomenon of GaN-based HFETs with a reduced electron velocity with certain gate voltages when the gate voltage becomes more negative [5]. It has been demonstrated experimentally that the electron velocity in GaN-based HFETs is not fixed but varies with gate-source voltage (V_{gs}) in the channel. MC simulations have been performed to study the electron velocity in AlGaN/GaN HFETs. Russo and Di Carlo proposed that the downscaling of source-gate length (L_{sg}) can enhance the electric field and the electron velocity in the source access region [6]. The velocity-field relationship

The associate editor coordinating the review of this manuscript and approving it for publication was Yue Zhang.

of AlGaN/GaN heterostructures was investigated by Yu and Brennan [7]. It was found that the peak velocity of 2DEG electron reaches 3×10^5m/s. However, these MC results cannot explain why the peak electron velocity of AlGaN/GaN HFETs is much lower than the 3×10^5m/s predicted by MC simulations and why the electron velocity decreases with a negative increase of V_{gs}. Our MC data is based on complete scattering mechanisms such as polarization Coulomb field (PCF) scattering, polar optical phonon (POP) scattering, acoustic deformation potential scattering, inter-valley phonon scattering, interface roughness scattering and piezoelectric scattering. Considering PCF scattering in the MC simulation can effectively explain the modulation effect of V_{gs} on the velocity. Pampori et al. [8] proposed a V_{gs}-dependent electron velocity model mainly considering POP scattering. However, this model cannot explain the experimental phenomenon that the electron velocity decreases as the gate voltage becomes more negative. An accurate velocity-field relationship model is a prerequisite for accurate modeling of the device and is essential to device experimentalists conducting oriented device design. This served as the motivation for our V_{gs}-dependent velocity field model and corresponding physics-based compact model.

As a result of fine-tuning the fitting parameters from the velocity-field model, the reported compact AlGaN/GaN HFET model corresponded highly with the experimental results [2], [3], [9], [10]. In practice, the errors in the velocity-field model approximation are ignored. However, there is a price for that—their physical meaning blur out, such as the saturation velocity. The specific scattering mechanism leading to the variation in the AlGaN/GaN HFET velocity-field relationship at different gate biases for different devices could not be clearly derived. Despite this simulation corresponding well with the experiment, it remains difficult to optimize the device characteristics based on the scattering mechanism and mobility model. In this paper, a 2-D AlGaN/GaN HFET compact model is proposed. Firstly, the velocity-field relationship of AlGaN/GaN HFETs with different gate voltages is obtained via MC simulation. Subsequently, a gate bias-dependent velocity-field model is established based on the velocity-field relationship of our prepared AlGaN/GaN HFET. The velocity-field relationship model fits well with the MC data, indicating that our model accurately describes the modulation of the electron velocity by V_{gs} variations. When we consider parasitic resistance and channel modulation effects, a compact AlGaN/GaN HFET model is derived, the parameters of which have clear physical meaning. This modeling approach preserves the correspondence between the velocity-field relationship parameters and the device, allowing us to more intuitively optimize the device performance using the transport and scattering mechanisms.

II. MONTE CARLO MODEL DESCRIPTION

Fig. 1(a) shows a schematic cross-section of the fabricated $Al_{0.21}Ga_{0.79}N$/GaN HFETs on a SiC substrate. The

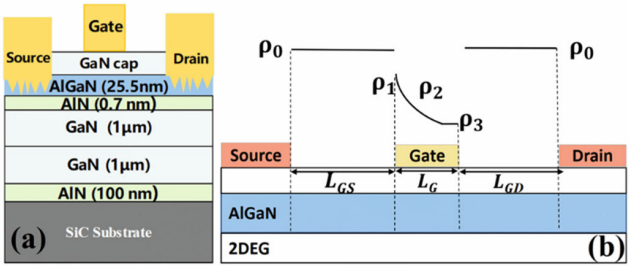

FIGURE 1. (a) Schematic cross-section of the AlGaN/GaN HFETs. (b) Schematic of the polarization charge density distribution at the AlGaN/AlN interface.

TABLE 1. Material parameters.

Parameters	Value	unit
Mass density	6100	kg/m^3
Acoustic phonon velocity	6600	m/s
Transverse sound velocity	2700	m/s
LO phonon. energy	92	meV
Inter-valley phonon. energy	65	meV

epitaxial layer from top to bottom consists of a 3 nm GaN cap layer, a 25.5 nm 21% AlGaN barrier layer, a 0.7 nm AlN interlayer layer, a 1μm GaN channel layer, a 1μm C-doped GaN buffer layer, and a 100 nm AlN nucleation layer. Devices with source-drain distances (L_{sd}) of 3.2 μm ($L_g = 0.2$ μm) and 3.35μm ($L_g = 0.35$ μm) are marked as sample 1 and sample 2. Sample 1 and 2 both have a gate width of 40 μm. The DC (I–V) measurements were taken using an Agilent B1500A semiconductor parameter analyzer.

We investigate the velocity-field relationship of AlGaN/GaN HFETs in the GaN channel via MC simulations, which consider five-energy valleys [11], [12], [13]. The five-energy valleys from low to high energy are Γ_1, U, Γ_3, M and K valleys. The non-parabolic constants are considered by the Kane model. Material parameters used in the MC simulations are shown in Table 1, which match very well with the reported data [14]. The acoustic deformation potential for GaN is 9.1 eV. And the intervalley deformation potential for GaN is 1×10^9 eV/cm which characterizes the strength of the scattering from the initial valley i to the final valley j. Complete scattering mechanisms such as polarization Coulomb field scattering, polar optical phonon scattering, acoustic deformation potential scattering, inter-valley phonon scattering, interface roughness scattering and piezoelectric scattering are included in our simulations.

We focus on PCF scattering in high field transport. Due to the variation of the gate and the drain biases, the inverse piezoelectric effect occurs. Non-uniform polarization charge distributions resulted in additional polarization charges (APCs). The differences between the polarization charge density in the gate region and the open region are defined as APCs. The APCs generate a scattering potential that scatter electrons in channel. The PCF scattering rate

is [15], [16], [17]:

$$\frac{1}{\tau_{\mathrm{PCF}}(E)} = \frac{Am^*}{2\pi\hbar^3}\int_{-\pi}^{\pi}\left|\frac{M_{k\to k'}}{S(q,T_e)}\right|^2(1-\cos\theta)\,d\theta. \quad (1)$$

where A is the 2-D normalization constant that converts the scattering rate per area, m^* is the electron effective mass in GaN, $\hbar$ is the Planck constant, θ is the scattering angle from k to k′, and S(q, Te) is the screening function, which can be written as [15], [16], and [17]:

$$S(q,T_e) = 1 + \frac{e^2F(q)\Pi(q,T_e,E)}{2\varepsilon_0\varepsilon_s q} \quad (2)$$

where F(q) is the form factor, ε_s is the static dielectric constant of GaN, and ε_0 represents the vacuum dielectric constant. q stands for the value change of wave vector, and Π(q, T_e, E) is the polarizability function. The scattering matrix element can be written as [15], [16], and [17]:

$$M_{k\to k'} = A^{-1}\int_0^{\infty}\Psi_k^*,(z)[\int_a^b dx\int_0^W V(x,y,z) \times \exp(-iq_x x - iq_y y)dy]\Psi_k(z)dz \quad (3)$$

where q_x, and q_y are the components of q in the x-direction and y-direction, $\psi_k^*(z)$ and $\psi_k(z)$ are the Fang–Howard variational wave function in the z-direction, W represents the gate width. In this equation, the integral interval (a, b) of x is the coordinate interval of the channel region in which the 2DEG is located in the x direction. Fig.1(b) shows a diagram of the polarization charge density distribution in the gate region with $V_{gs} = 0$V and $V_{ds} = 6$V. We approximated the simulation by dividing the gate region into several grids. Each grid corresponds to the coordinates (x_1, x_2) and a polarization charge density ρ_2. We determined the polarization charge density ρ_0 in the gate-source and gate-drain regions. We determined ρ_1 and ρ_3 at the leftmost endpoint and the rightmost endpoint of the gate. According to the PCF scattering definition, the PCF additional scattering potential is written as [17]:

$$\begin{aligned}
&V(x,y,z)\\
&= \frac{-e}{4\pi\varepsilon_s\varepsilon_0}\Bigg(\int_{-L_{GS}-\frac{L_G}{2}}^{-\frac{L_G}{2}} dx'\int_0^W \frac{\rho_0-\rho_2}{\sqrt{(x-x')^2+(y-y')^2+(z)^2}}dy'\\
&+\int_{+\frac{L_G}{2}}^{L_{GD}+\frac{L_G}{2}} dx'\int_0^W \frac{\rho_0-\rho_2}{\sqrt{(x-x')^2+(y-y')^2+(z)^2}}dy'\\
&+\int_{-\frac{L_G}{2}}^{X_1} dx'\int_0^W \frac{\frac{(\rho_3-\rho_1)x'}{L_G}+\frac{(\rho_3+\rho_1-2\rho_2)}{2}}{\sqrt{(x-x')^2+(y-y')^2+(z)^2}}dy'\\
&+\int_{X_2}^{\frac{L_G}{2}} dx'\int_0^W \frac{\frac{(\rho_3-\rho_1)x'}{L_G}+\frac{(\rho_3+\rho_1-2\rho_2)}{2}}{\sqrt{(x-x')^2+(y-y')^2+(z)^2}}dy'\Bigg) \quad (4)
\end{aligned}$$

where the leftmost endpoint coordinate of each mesh is x_1, and the rightmost endpoint coordinate of each mesh is x_2. e represents the quantity of electric charge. PCF scattering rate can be calculated via Equations (1), (2), (3) and (4). And other scattering rate formulations primarily refer to the scattering rate form in the literature [18]. Our MC simulation is based on a fixed potential [17], [19].

Below we present a brief introduction of the method used to study the electron transport.

1) Initially, we determined the potential and electric field distribution within the GaN channel using the analytical solution to the Poisson equation [17].

2) Subsequently, we utilized the lateral electric field profile and conducted Monte Carlo simulations to simulate the electron velocity within the channel.

We employed Monte Carlo simulation by partitioning the channel into several grids and assuming uniform electron density and electric field within each grid. Employing the analytical solution of the Poisson equation, we obtained the electric field and electron density distribution at various grids. Subsequently, we calculated all scattering rates for these grids. Using the electric field determined for each grid, we employed the Monte Carlo method to derive the electron velocity in different grids. We then extracted the electron velocity and electric field to obtain data for the velocity-field relationship. More details about the MC simulation can be found in Ref [17].

III. VELOCITY- FIELD RELATIONSHIP MODEL AND I-V MODEL

Fig. 2, and 4 show the velocity-field characteristic MC data considering PCF scattering for Samples 1 and 2. The average velocity in the gate of sample 1 decreases from 1.35×10^5 m/s at $V_{gs} = 0$V to 1.21×10^5 m/s at $V_{gs} = -3$ V, and the average velocity in the gate of sample 2 decreases from 1.31×10^5 m/s at $V_{gs} = 0$V to 1.2×10^5 m/s at $V_{gs} = -3$ V. The electron velocity decreases continuously with the decrease of the gate bias. Due to the inverse piezoelectric effect, the polarization charges in the gate region decrease as the negative gate bias increases. The difference between the polarization charges in the open and gate regions increases. As the APCs increases, the PCF scattering and total scattering rate are increased, resulting in a decrease in electron velocity. We proposed that the gate bias has a modulating effect on the electron velocity which can be attributed to PCF scattering.

To compare the previous velocity-field relation model to our new velocity-field relation model, calculations of the velocity-field characteristics for Samples 1 and 2 were made using the above two models, respectively. We observed the Negative Differential Resistance (NDR) phenomenon in Figs. 2, 4. So, for the previous model, we refer to Equations (5) and (6) in the literatures [2] and [20] to describe the velocity-field relationship.

$$\mu_0 = \mu_{\min} + \frac{\mu_{\max}-\mu_{\min}}{1+(\frac{n}{n_{ref}})^{\alpha}} \quad (5)$$

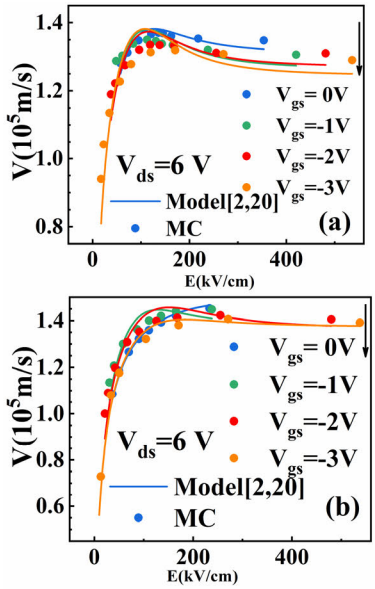

FIGURE 2. (a) Model [2], [20] of the velocity-field characteristics and MC data of the velocity-field characteristics in sample 1. (b) Model [2], [20] of the velocity-field characteristics and MC data of the velocity-field characteristics in sample 2.

TABLE 2. Parameters used in the model [2], [20].

parameter	description	Sample1	Sample2
$\mu(cm^2/V.s)$	Mobility	869	869
$V_{sat}(10^5m/s)$	Saturation velocity (V_{gs}=0V,-1V,-2V,-3V)	1.309,1.26, 1.26 ,1.24	1.2,1.37, 1.361.37
E_t(kV/cm)	Critical electric field (V_{gs}=0V,-1V,-2V,-3V)	80,81,80,85	271,80,100,93.6
a	Velocity parameter (V_{gs}=0V,-1V,-2V,-3V)	4.19,4.09, 4.14,4.04	14.82,3.98, 5.08,5.11

$$V(E) = \frac{\mu_0 E + v_{sat}(\frac{E}{E_t})^4}{1 + (\frac{E}{E_t})^4 + a(\frac{E}{E_t})^4} \tag{6}$$

where μ_0 is the low field mobility, μ_{min} is the mobility in highly doped GaN, μ_{max} is the mobility in unintentionally doped GaN, n_{ref} is the carrier concentration at which the mobility is halfway between μ_{min} and μ_{max}, α is a measure of how quickly the mobility changes from μ_{min} to μ_{max}, n is the total doping density. μ_0 is determined by Equation (5). The three parameters v_{sat}, a, E_t are determined by fitting Monte Carlo simulations of AlGaN/GaN HFETs with different V_{gs}. These parameters extracted from our MC data are shown in table 2. The comparison between the previous velocity-field relation model and the MC data of the velocity-field characteristics considering PCF scattering for sample 1 and sample 2 is depicted in Fig.2. We find that this model [2], [20] has some defects and it does not describe well the experimental phenomenon that the channel electron velocity of GaN HFETs keeps decreasing significantly with the negative increase of V_{gs}. Previous models [2], [20] have never considered PCF scattering.

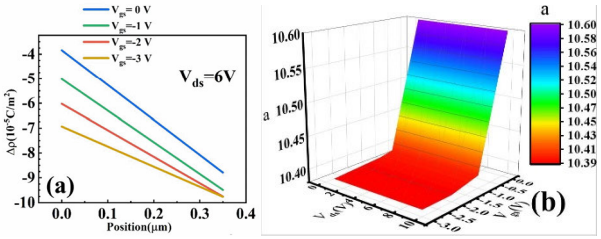

FIGURE 3. (a) The additional polarization charge density distribution at the AlGaN/AlN interface of AlGaN/GaN HFETs in sample 2. (b) The parameter a as a function of V_{gs} and V_{ds}.

Our new model was improved based on Equation (6). As shown in **Fig. 3(a)**, the additional polarization charge distribution of the AlGaN barrier layer is significantly affected by V_{gs} variations [15], [16], [21], [22], [23], [24]. PCF scattering plays a dominant role in the phenomenon that electron velocity decreases continuously as the gate bias decreases in AlGaN/GaN HFETs. Due to the inverse piezoelectric effect, the polarization charges in the gate region decrease as the negative gate bias increases. The difference between the polarization charges in the gate and open regions continuously increases. Since the PCF scattering is strengthened, the electron velocity is continuously reduced. We find a correlation between V_{gs} and parameter a. Parameters such as the polarization charge density associated with PCF scattering were introduced to describe the dependence of V_{gs} on the velocity field parameter a.

Therefore, the parameter a is purposed, which is an empirical expression with physical meaning based on the MC data for a number of AlGaN/GaN HFETs at different biases:

$$a = \varepsilon_s + \frac{\rho_3 - \rho_0}{\rho_1 - \rho_0} \tag{7}$$

where ε_s is the relative permittivity of the barrier layer, ρ_1 is the polarization charge density at the leftmost endpoint of the gate, ρ_3 is the polarization charge density at the rightmost endpoint of the gate, and ρ_0 is the polarization charge density in the gate-source and gate-drain regions. As illustrated in Fig.3(b), we calculated the parameter a as a function of V_{gs} and V_{ds} for sample 1 based on Equation (7).

According to the approximation [25], we find that $\mu_0 = (v_{sat}(1+a))/E_t$, so we obtain Equation (8).

$$v(E) = \frac{v_{sat}(1 + \varepsilon_s + \frac{\rho_3 - \rho_0}{\rho_1 - \rho_0})e_x}{1 + (\varepsilon_s + \frac{\rho_3 - \rho_0}{\rho_1 - \rho_0})e_x} \tag{8}$$

We determined the polarization charge density ρ_0 in the gate-source and gate-drain regions. We determined ρ_1 and ρ_3 at the leftmost endpoint and the rightmost endpoint of the gate. By solving the Poisson equation, we obtained the potential V_1 at the leftmost end of the gate and the potential V_3 at the rightmost end of the gate. According to the APCs as a function of the channel bias [17], each channel bias corresponds to a polarization charge density. ρ_1 and ρ_3 are determined by potentials V_1 and V_3. We extracted E_t and v_{sat}

TABLE 3. Parameters used in the our new model.

parameter	description	Sample1	Sample2
V_{th}(V)	Threshold voltage	-3.6	-3.7
d(nm)	Barrier layer thickness	25.5	25.5
$V_{sat}(10^5 m/s)$	Saturation velocity (V_{gs}=0V,-1V,-2V,-3V)	1.33,1.31, 1.3, 1.28	1.43,1.41, 1.39,1.36
E_t(kV/cm)	Critical electric field (V_{gs}=0V,-1V,-2V,-3V)	82,60, 79,85	183,122, 120,150
$\varepsilon_s + \frac{\rho_3 - \rho_0}{\rho_1 - \rho_0}$	Velocity parameter (V_{gs}=0V,-1V,-2V,-3V)	10.6,10.4, 10.39,10.39	11.68,11.28, 11.01,10.8

by a least squares fit of Equation (8) to velocity data from Monte Carlo calculations. These parameters extracted from our MC data are shown in Table 3. We compared the model data based on Equations (7) and (8) with the Monte Carlo data, as shown in Fig.4. Fig. 4(a) and (b) show the velocity-field relationship for AlGaN/GaN HFETs with different V_{gs}, demonstrating excellent agreement between our model and the MC data. The MC data can be effectively modeled by our new model based on the parameter a and adjustable parameters E_t and v_{sat}. The new model can satisfactorily describe that the more negative the V_{gs}, the lower the channel electron velocity. It can also describe the effect of V_{gs} on PCF scattering compared with the previous model [2], [20] (Equations 5,6).

To better examine the connection between V_{ds} and the velocity-field relationship, we also calculated the velocity-field relationship for Sample 1 at $V_{gs} = 0$V, $V_{ds} = 8$V, and $V_{ds} = 10$V. We compared MC data with our new velocity-field relationship model in Fig.4(c) and (d). The extracted parameters are the same as $V_{gs} = 0$Vand $V_{ds} = 6$V in Table 3. The analysis results showed that the electric field is effectively increased when V_{ds} increases, but it has a weak influence on the velocity-field relationship. Therefore, we concluded that the velocity-field relationship is independent of the V_{ds}.

To better understand the meaning of Equations (7) and (8), we calculated the velocity-field relationship for Sample 1 at $V_{ds} = 0$V and $V_{gs} = 0$V without considering PCF scattering and compared it with our velocity-field relationship model in Fig. 5(a). As illustrated, the electron velocity in Fig. 5(a) is much larger than the electron velocity in Fig. 4(a)-(d), which can be attributed to the absence of PCF scattering [17]. When the gate and drain bias are set as zero, ρ_3 and ρ_1 are equal to ρ_0. Then, the second term of the right hand of Eq. (7) is calculated to 1 and Eq. (7) $= \varepsilon_s + 1$. When the denominator of the second term of Eq. (7) is very small, the drain bias and gate bias are small. The numerator of the second term of Eq. (7) will also be small and be in the same order of magnitude as the denominator, so the second term of Eq. (7) is equal to 1 at $V_{ds} = 0$V and $V_{gs} = 0$V. As illustrated in Fig. 5(a), the MC data is still in good agreement with the model data. The results show that Equations (7) and (8) can describe the velocity-field relationship for AlGaN/GaN HFETs without PCF scattering. We calculated the velocity-field relationship

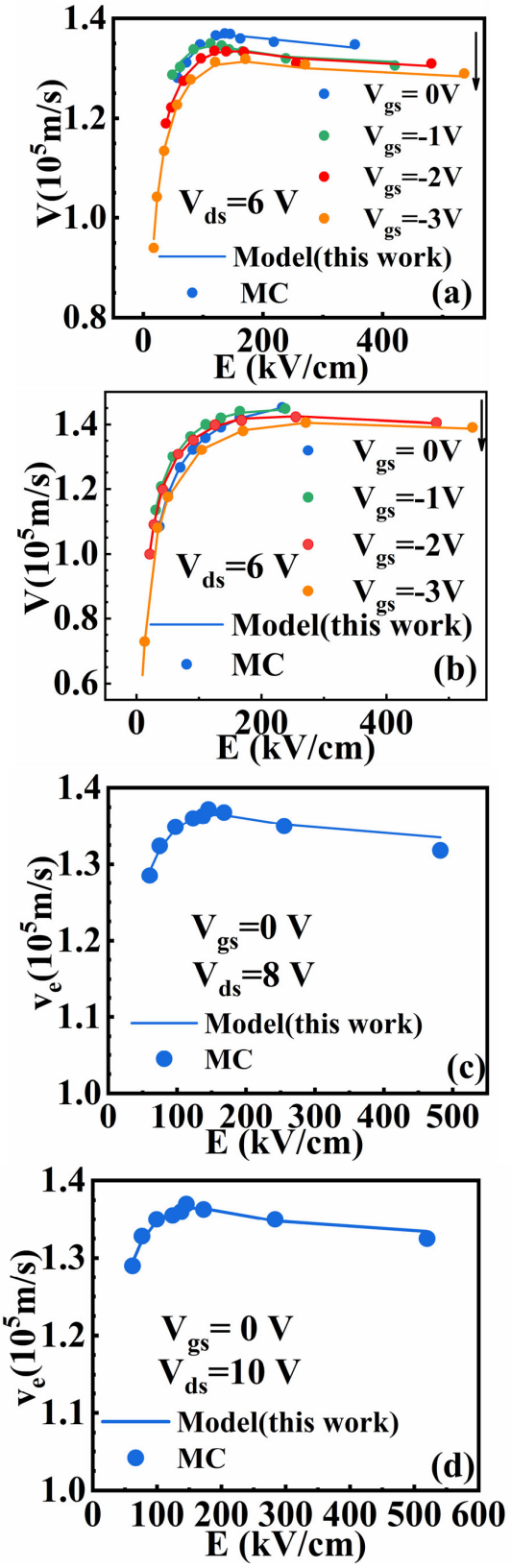

FIGURE 4. (a) Model of the velocity-field characteristics and their MC data in Sample 1; (b) Model and MC data in Sample 2. (c) Model and MC data in Sample 1 at $V_{ds} = 8$ V, $V_{gs} = 0$ V. (d) Model and MC data in Sample 1 at $V_{ds} = 10$ V, $V_{gs} = 0$ V.

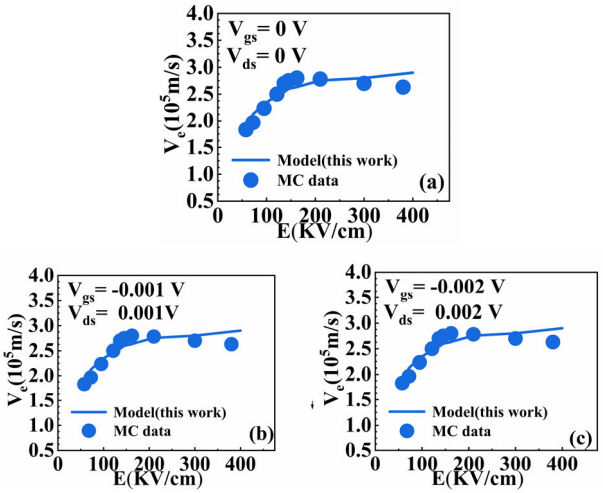

FIGURE 5. Model of the velocity-field characteristics and MC data of the velocity-field characteristics for Sample 1 at (a) V_{ds} = 0 V, V_{gs} = 0 V. (b) V_{ds} = 0.001 V, V_{gs} =−0.001 V and (c) V_{ds} = 0.002 V, V_{gs} =−0.002 V.

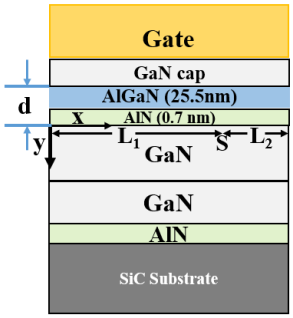

FIGURE 6. Cross-sectional view of the fabricated AlGaN/GaN HFET. L denotes the gate length. L_1 and L_2 are the lengths of the low-field and saturation regions in the channel, respectively. d denotes the barrier layer thickness. S is the onset point of the velocity saturation. Y=0 is in the heterointerface.

for sample 1 at V_{ds} = 0.001 V, V_{gs} = −0.001 V and V_{ds} = 0.002 V, V_{gs} = −0.002 V and compared it with our velocity-field relationship model in Fig. 5(b)-(c). When V_{ds}, and V_{gs} are small, the transverse channel potentials do not conduct. ρ_3 and ρ_1 are smaller than ρ_0, and ρ_3 minus ρ_0 is equal to ρ_3 minus ρ_0, hence Eq. (7) = ε_s+1. Good agreement between the MC data and the model data shows that the velocity-field features around V_{ds} = V_{gs} = 0V still satisfy the calculations in equations 7 and 8, as confirmed in Fig.5(b)-(c).

Drawing on the derivation from References [2] and [25], we obtain the I-V equation. The current is calculated from I = Wqv(x)n_s (x).

In the linear region, the electron concentration can be obtained based on the charge control model. When E<E_t, our velocity-field (v(E)) model can be simplified as:

$$\mathrm{V(E)} = \frac{v_{sat}(1+\varepsilon_s+\frac{\rho_3-\rho_0}{\rho_1-\rho_0})e_x}{1+(\varepsilon_s+\frac{\rho_3-\rho_0}{\rho_1-\rho_0})e_x} \tag{9}$$

where a = ε_s + (ρ_3−ρ_0)/ (ρ_1−ρ_0), e_x = E(x)/E_t. We write n_s and v(E) to the current.

$$I = \lambda E_t \frac{e_x}{1+(\varepsilon_s+\frac{\rho_3-\rho_0}{\rho_1-\rho_0})e_x}(V_{GT}-V(x)) \tag{10}$$

where $\lambda = (w\varepsilon_s v_{sat}$ (1+a)/E_t/d), V_{GT} = V_G-V_{th}.

According to the equation transformation, we obtain

$$\frac{I}{\lambda E_t}\frac{E_t+(\varepsilon_s+\frac{\rho_3-\rho_0}{\rho_1-\rho_0})\frac{dV(x)}{dx}}{\frac{dV(x)}{dx}} = (V_{GT}-V(x)) \tag{11}$$

$$\frac{I}{\lambda E_t}(E_t dx+(\varepsilon_s+\frac{\rho_3-\rho_0}{\rho_1-\rho_0})dV(x)) = (V_{GT}-V(x))dV(x) \tag{12}$$

Integrating along the channel from the source to the drain, the current in the linear region can be obtained as follows:

$$I = \frac{\lambda E_t(2V_{GT}-V_{DS})V_{DS}}{2(E_t L+(\varepsilon_s+\frac{\rho_3-\rho_0}{\rho_1-\rho_0})V_{DS})} \tag{13}$$

The parasitic source and drain resistance have a significant impact on the HFET device performance. The relationship between the intrinsic and extrinsic gate-source and drain–source voltages are shown as:

$$V_{GS} = V_{gs} - IR_s \tag{14}$$

$$V_{DS} = V_{ds} - I(R_s+R_d) \tag{15}$$

Equation (14) and (15) are then substituted into Equation (13). We obtain:

$$I = \frac{4V_{gt}V_{ds}-2V_{ds}^2}{\sqrt{B^2-4D}+B} \tag{16}$$

where R_n=1/(λE_t)

$$B = (2(\varepsilon_s+\frac{\rho_3-\rho_0}{\rho_1-\rho_0})R_n V_{ds}+2E_t L R_n+2V_{gt}(R_s+R_d)) \tag{17}$$

$$D = (R_d-R_s-2(\varepsilon_s+\frac{\rho_3-\rho_0}{\rho_1-\rho_0})R_n)(R_d+R_s)(-2V_{gt}V_{ds}+V_{ds}^2) \tag{18}$$

At V_{ds} = V_{dsat}, the Equation can be derived from Equation (10):

$$\frac{I}{\lambda E_t}\frac{1+(\varepsilon_s+\frac{\rho_3-\rho_0}{\rho_1-\rho_0})e_x}{e_x} = (V_{GT}-V(x)) \tag{19}$$

we divide both sides of the equation by e_x^2, and then integrate e from the source to any position in the channel to obtain:

$$\frac{I}{\lambda E_t}\int_{e(0)}^{e(x)}\frac{1+(\varepsilon_s+\frac{\rho_3-\rho_0}{\rho_1-\rho_0})e_x}{e_x^3}de = \int_{e(0)}^{e(x)}\frac{V_{GT}-V(x)}{e_x^2}de \tag{20}$$

We obtain the following expression by integration:

$$\frac{I}{\lambda E_T}(\frac{1}{2e_0^2}-\frac{1}{2e_x^2}) = E_t x \tag{21}$$

By substituting x=0, V(x)=0, we obtain

$$I_{sat} = \frac{V_{GT}\lambda E_T e_{0sat}}{1+(\varepsilon_s+\frac{\rho_3-\rho_0}{\rho_1-\rho_0})e_{0sat}} \tag{22}$$

Bringing x=L, e_{Lsat}=1 into Equation (19), we get

$$e_{0sat} = \frac{\sqrt{(2(\varepsilon_s+\frac{\rho_3-\rho_0}{\rho_1-\rho_0})E_tL+V_{GT})V_{GT}+E_t^2L^2}-E_tL}{2(\varepsilon_s+\frac{\rho_3-\rho_0}{\rho_1-\rho_0})E_tL+V_{GT}} \tag{23}$$

$$V_{dsat} = V_{GT} - \frac{I_{dsat}(1+(\varepsilon_s+\frac{\rho_3-\rho_0}{\rho_1-\rho_0}))}{\lambda E_t} \tag{24}$$

When $V_{ds} > V_{dsat}$, the device is in the velocity saturation region and the channel modulation effect should be considered.

In the high field region, the 2-D Poisson equation is solved in the AlGaN layer near the drain end of the channel.

$$\frac{\partial^2 V_C(x',y)}{\partial x'^2}+\frac{\partial^2 V_C(x',y)}{\partial y'^2} = -\frac{qN_d(y)}{\varepsilon} \tag{25}$$

where $0< x' < L_2$=L-L_1, N_d (y) is the doping concentration of the barrier layer in Fig 6.

The solution of Equation (25) can be written as the sum of the solutions of a 1-D Poisson equation and a 2-D Laplace Equation [9].

$$V_c(x',y) = \psi(y)+\varphi(x',y) \tag{26}$$

$$\frac{\partial^2\psi(y)}{\partial y^2} = -\frac{qN_d(y)}{\varepsilon} \tag{27}$$

$$\frac{\partial^2\varphi(x',y)}{\partial x'^2}+\frac{\partial^2\varphi(x',y)}{\partial y'^2} = 0 \tag{28}$$

For the 1-D Poisson equation, the bottom of the conduction band in GaN is where the origin of the potential is defined, and Equations (29) and (30) are the boundary conditions.

$$\psi(y)|_{y=-d} = V_{gs}-\phi_B \tag{29}$$

$$\frac{\partial\psi(y)}{\partial y}|_{y=0} = \frac{-qn_{sat}}{\varepsilon} \tag{30}$$

where n_{sat} is the 2DEG electron density at point S,φ_B is the barrier height of the Schottky gate.

We integrate Equation (27) from the heterojunction (y = 0) to any point in the AlGaN layer:

$$\frac{\partial\psi(y)}{\partial y}-\frac{\partial\psi(0)}{\partial y} = -\frac{q\int_0^y N_d(y)dy}{\varepsilon} \tag{31}$$

We bring Equation (30) into Equation (31), and then integrate along y from -d to y

$$\psi(y) = V_{gs}-\phi_B-\frac{q}{\varepsilon}n_{sat}(y+d)-\frac{q}{\varepsilon}\int_{-d}^{y}dy\int_0^y N_d(y)dy \tag{32}$$

According to the separation of variables method, the Equation (28) solution has the following form.

$$\varphi(x',y) = (A\sinh(kx')+B\cosh(kx'))(C\sinh(ky)+B\cosh(ky)) \tag{33}$$

The boundary conditions for the 2D Laplace equation are

$$\varphi(0,y)=0,\ \frac{\delta\varphi(0,0)}{\delta x'} = E_t$$
$$\varphi(x',y)=0,\ \frac{\delta\varphi(0,0)}{\delta y} = 0. \tag{34}$$

The solution of the 2D Laplace equation is

$$\varphi(x',y) = \frac{2dE_t}{\pi}\sinh(\frac{\pi}{2d}x')\cosh(\frac{\pi}{2d}y) \tag{35}$$

$$V_c(x',y) = \frac{2dE_t}{\pi}\sinh(\frac{\pi}{2d}x')\cosh(\frac{\pi}{2d}y)+V_{gs}-\phi_B - \frac{q}{\varepsilon}n_{sat}(y+d)-\frac{q}{\varepsilon}\int_{-d}^{y}dy\int_0^y N_d(y)dy \tag{36}$$

y=0 is brought into Equation (36). The potential is continuous.

$$V_c(x') = \frac{2dE_t}{\pi}\sinh(\frac{\pi}{2d}x')+V_{gs}-\phi_B-\frac{q}{\varepsilon}n_{sat}d \tag{37}$$

$$V_c(x') = p\sinh(\frac{\pi}{2d}x')+V_{gs}-\phi_B-\frac{q}{\varepsilon}n_{sat}d \tag{38}$$

The potential drop in the high field region can be expressed as:

$$V_H(x') = V_H(L_2)-V_H(0) = p\sinh(\frac{\pi}{2d}x') \tag{39}$$

We introduce an adjustable eigenvalue p, whose adjustability stems from the uncertainty of the boundary conditions. p is affected by the gate bias and can describe the effect of the gate bias on the length of the saturation region length and conductance in the velocity saturation region. By fine-tuning the p-value at different V_{gs}, the model can effectively describe the channel modulation effect in GaN HFETs and achieve a high correlation between the experimental and simulated current in the saturation region.

Bringing x = 0 into Equation (10), V(0) = 0

$$I(1+(\varepsilon_s+\frac{\rho_3-\rho_0}{\rho_1-\rho_0})e_0) = \lambda E_t e_0 V_{gt} \tag{40}$$

Bringing x = L_1 into Equation (10), e_{L1}=1

$$I(1+(\varepsilon_s+\frac{\rho_3-\rho_0}{\rho_1-\rho_0})e_0) = \lambda E_t(V_{gt}-V_{L1}) \tag{41}$$

Bringing x = L_1 into Equation (21), e_{L1} = 1

$$I(\frac{1}{2e_0^2}-\frac{1}{2}) = \lambda E_t E_t L_1 \tag{42}$$

According to Equations (39), (40), (41), and (42), we obtain

$$\begin{cases} I(1+(\varepsilon_s+\frac{\rho_3-\rho_0}{\rho_1-\rho_0})e_0) = \lambda E_t e_0 V_{gt} \\ I(1+(\varepsilon_s+\frac{\rho_3-\rho_0}{\rho_1-\rho_0})e_0) = \lambda E_t(V_{gt}-V_{L1}) \\ I(\frac{1}{2e_0^2}-\frac{1}{2}) = \lambda E_t E_t L_1 \\ V_{L1}+pE_t\sinh(\frac{L-L_1}{p}) = V_{DS} \end{cases} \tag{43}$$

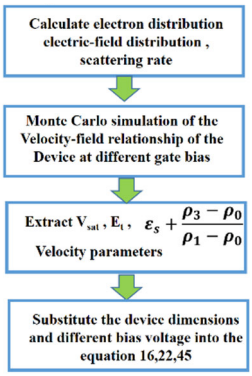

FIGURE 7. Flowchart of the I-V model calculation sequence.

Equation (43) can be simplified to obtain:

$$V_{GT}\left(1-\frac{(1+(\varepsilon_s+\frac{\rho_3-\rho_0}{\rho_1-\rho_0}))e_0}{1+(\varepsilon_s+\frac{\rho_3-\rho_0}{\rho_1-\rho_0})e_0}\right) + pE_t\sinh\left(\frac{L-\frac{V_{GT}(1-e_0^2)}{2e_0(1+(\varepsilon_s+\frac{\rho_3-\rho_0}{\rho_1-\rho_0})e_0)E_t}}{p}\right) = V_{DS} \tag{44}$$

We can obtain:

$$\begin{cases} I = \dfrac{V_{GT}\lambda E_t e_0}{1+(\varepsilon_s+\frac{\rho_3-\rho_0}{\rho_1-\rho_0})e_0} \\ V_{GT}\left(1-\dfrac{(1+(\varepsilon_s+\frac{\rho_3-\rho_0}{\rho_1-\rho_0}))e_0}{1+(\varepsilon_s+\frac{\rho_3-\rho_0}{\rho_1-\rho_0})e_0}\right) \\ \quad + pE_t\sinh\left(\dfrac{L-\frac{V_{GT}(1-e_0^2)}{2e_0(1+(\varepsilon_s+\frac{\rho_3-\rho_0}{\rho_1-\rho_0})e_0)E_t}}{p}\right) = V_{DS} \\ V_{DS} = V_{ds} - I(R_s+R_d) \\ V_{GS} = V_{gs} - IR_s \end{cases} \tag{45}$$

The calculation of this model can be summarized in the four steps shown in Fig. 7.

IV. RESULTS AND DISCUSSION

Following the steps in **Fig. 7**, we simulated the output and transfer characteristics of two different gate-length devices to validate the accuracy of the velocity-field relationship model and the compact model. Sample 1 had a gate length of 0.2μm, and Sample 2 had a gate the gate length of 0.35μm. The parameters used in the modeling are displayed in Table 3.

A clear channel modulation effect is observed in the high current region in **Fig. 8(a)**. We consider that p is an eigenvalue subject to the gate voltage modulation effect in Equation 45, which can describe the effect of the gate voltage on the length and conductance of the saturation region. Our model accurately reveals this experimental phenomenon.

We have compared our new v(E) model with the old v(E) model (Eq.6). Specifically, we utilized the old v(E) model (Eq. 6) to extract the parameters from the Monte Carlo (MC) data of the two devices. Subsequently, we employed

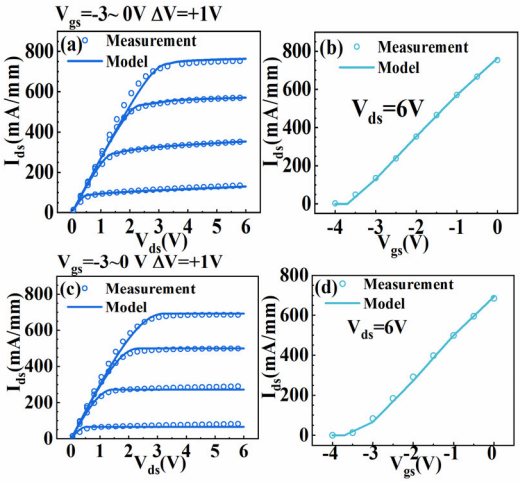

FIGURE 8. Calculations and measurements based on our v(E) model. (a) Calculated and measured I–V characteristics for sample 1. (b) Calculated and measured transfer characteristics for sample 1. (c) Calculated and measured I–V characteristics for sample 2. (d) Calculated and measured transfer characteristics for sample 2.

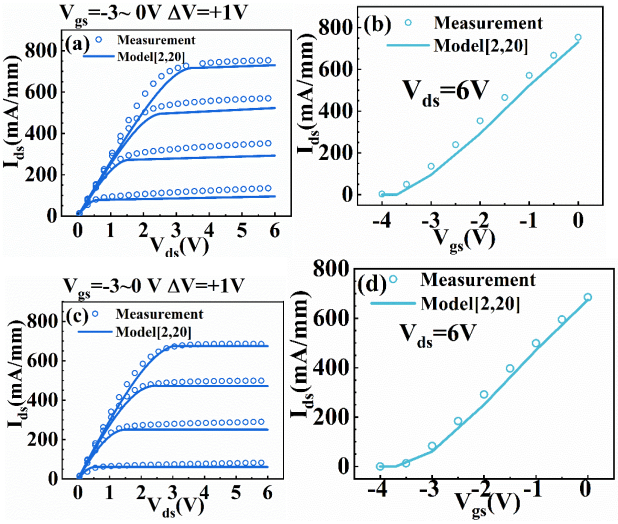

FIGURE 9. Calculations and measurements based on the old v(E) model [2], [20]. (a) Calculated and measured I–V characteristics for sample 1. (b) Calculated and measured transfer characteristics for sample 1. (c) Calculated and measured I–V characteristics for sample 2. (d) Calculated and measured transfer characteristics for sample 2.

these extracted parameters to calculate the output and transfer curves for both devices. Our analysis revealed that the output and transfer characteristic curves for both devices obtained from the old v(E) model (Eq. 6) mismatch the outcomes of the experiments in **Fig.9**. While, a better agreement of the I-V and DC transfer characteristics obtained from our new v(E) model with the experiments can be found in Fig.8. It can mainly be attributed to the accuracy of our modified bias-dependent velocity-field relationship model. **Fig. 8** shows the model scalability with the gate length, further demonstrating that the velocity-field model considers the dependence on gate bias in the TCAD model and the compact model is closer to the actual physical effect. **Figures 8(b)** and **(d)** show that

the transfer characteristics of our simulations are in good agreement with the tests. This demonstrates that our model can accurately predict the transconductance of the device.

Our model obtains the velocity-field relationship via MC simulation. We extract the velocity parameters according to Equation (8), incorporate the device and velocity parameters into our compact model, and finally obtain the simulation results. This modeling approach ensures that the velocity-field parameters are correlated with the fabricated AlGaN/GaN HFET and so the issue of missing physical meaning caused by the fitted velocity-field model parameters can be avoided. Through the above explanation, we also discovered that both the hot phonon effect and PCF scattering have a significant impact on the AlGaN/GaN HFET conductance modulation. Consequently, the drift velocity can be effectively improved by adjusting the PCF scattering and hot phonon effects.

V. CONCLUSION

AlGaN/GaN HFET gate bias-dependent velocity-field relationship model and compact current models are developed. The physical mechanism of electron velocity modulation by gate bias in AlGaN/GaN HFET is proposed. Our velocity-field relation model, which considers PCF scattering, satisfactorily reflects the decreasing electron velocity dependence as the gate voltage increases negatively. Our accurate velocity field model is a prerequisite for the accurate modeling of the device and is of significant importance to device experimentalists conducting oriented device design. A good agreement between the simulated I-V and transfer characteristics with the experiments validates the accuracy of our compact model. Our model achieves accurate I-V modeling by extracting the velocity-field parameters through MC simulation. This approach preserves the physical meaning of the parameters while effectively reducing the fitting parameters.

REFERENCES

[1] W. Deng, J. Huang, X. Ma, and J. J. Liou, "An explicit surface potential calculation and compact current model for AlGaN/GaN HEMTs," *IEEE Electron Device Lett.*, vol. 36, no. 2, pp. 108–110, Feb. 2015, doi: 10.1109/LED.2015.2388706.

[2] M. Li and Y. Wang, "2-D analytical model for current–voltage characteristics and transconductance of AlGaN/GaN MODFETs," *IEEE Trans. Electron Devices*, vol. 55, no. 1, pp. 261–267, Jan. 2008, doi: 10.1109/TED.2007.911076.

[3] X. Cheng, M. Li, and Y. Wang, "Physics-based compact model for AlGaN/GaN MODFETs with close-formed I–V and C–V characteristics," *IEEE Trans. Electron Devices*, vol. 56, no. 12, pp. 2881–2887, Dec. 2009, doi: 10.1109/TED.2009.2030722.

[4] B. Romanczyk, M. Guidry, X. Zheng, H. Li, E. Ahmadi, S. Keller, and U. K. Mishra, "Bias-dependent electron velocity extracted from N-Polar GaN deep recess HEMTs," *IEEE Trans. Electron Devices*, vol. 67, no. 4, pp. 1542–1546, Apr. 2020, doi: 10.1109/TED.2020.2973081.

[5] J. H. Leach, C. Y. Zhu, M. Wu, X. Ni, X. Li, J. Xie, Ü. Özgür, H. Morkoç, J. Liberis, E. Šermukšnis, A. Matulionis, T. Paskova, E. Preble, and K. R. Evans, "Effect of hot phonon lifetime on electron velocity in InAlN/AlN/GaN heterostructure field effect transistors on bulk GaN substrates," *Appl. Phys. Lett.*, vol. 96, no. 13, Mar. 2010, Art. no. 133505, doi: 10.1063/1.3358392.

[6] S. Russo and A. Di Carlo, "Influence of the source–gate distance on the AlGaN/GaN HEMT performance," *IEEE Trans. Electron Devices*, vol. 54, no. 5, pp. 1071–1075, May 2007, doi: 10.1109/TED.2007.894614.

[7] T.-H. Yu and K. F. Brennan, "Monte Carlo calculation of two-dimensional electron dynamics in GaN–AlGaN heterostructures," *J. Appl. Phys.*, vol. 91, no. 6, pp. 3730–3736, Mar. 2002, doi: 10.1063/1.1448889.

[8] A. U. H. Pampori, S. A. Ahsan, R. Dangi, U. Goyal, S. K. Tomar, M. Mishra, and Y. S. Chauhan, "Modeling of bias-dependent effective velocity and its impact on saturation transconductance in AlGaN/GaN HEMTs," *IEEE Trans. Electron Devices*, vol. 68, no. 7, pp. 3302–3307, Jul. 2021, doi: 10.1109/TED.2021.3078717.

[9] S. Haldar and R. S. Gupta, "2-D analytical model for current–voltage characteristics and output conductance of AlGaN/GaN MODFET," *Microw. Opt. Technol. Lett.*, vol. 29, no. 2, pp. 117–123, Apr. 2001, doi: 10.1002/mop.1102.

[10] S. Khandelwal, C. Yadav, S. Agnihotri, Y. S. Chauhan, A. Curutchet, T. Zimmer, J.-C. De Jaeger, N. Defrance, and T. A. Fjeldly, "Robust surface-potential-based compact model for GaN HEMT IC design," *IEEE Trans. Electron Devices*, vol. 60, no. 10, pp. 3216–3222, Oct. 2013, doi: 10.1109/TED.2013.2265320.

[11] T. Sadi and R. W. Kelsall, "Theoretical study of electron confinement in submicrometer GaN HFETs using a thermally self-consistent Monte Carlo method," *IEEE Trans. Electron Devices*, vol. 55, no. 4, pp. 945–953, Apr. 2008, doi: 10.1109/TED.2008.916677.

[12] T. Sadi, R. W. Kelsall, and N. J. Pilgrim, "Investigation of self-heating effects in submicrometer GaN/AlGaN HEMTs using an electrothermal Monte Carlo method," *IEEE Trans. Electron Devices*, vol. 53, no. 12, pp. 2892–2900, Dec. 2006, doi: 10.1109/TED.2006.885099.

[13] J. D. Albrecht, R. P. Wang, P. P. Ruden, M. Farahmand, and K. F. Brennan, "Electron transport characteristics of GaN for high temperature device modeling," *J. Appl. Phys.*, vol. 83, no. 9, pp. 4777–4781, May 1998, doi: 10.1063/1.367269.

[14] U. V. Bhapkar and M. S. Shur, "Monte Carlo calculation of velocity-field characteristics of Wurtzite GaN," *J. Appl. Phys.*, vol. 82, no. 4, pp. 1649–1655, Aug. 1997, doi: 10.1063/1.365963.

[15] C. Luan, Z. Lin, Y. Lv, J. Zhao, Y. Wang, H. Chen, and Z. Wang, "Theoretical model of the polarization Coulomb field scattering in strained AlGaN/AlN/GaN heterostructure field-effect transistors," *J. Appl. Phys.*, vol. 116, no. 4, p. 44507, Jul. 2014, doi: 10.1063/1.4891258.

[16] P. Cui, H. Liu, W. Lin, Z. Lin, A. Cheng, M. Yang, Y. Liu, C. Fu, Y. Lv, and C. Luan, "Influence of different gate biases and gate lengths on parasitic source access resistance in AlGaN/GaN heterostructure FETs," *IEEE Trans. Electron Devices*, vol. 64, no. 3, pp. 1038–1044, Mar. 2017, doi: 10.1109/TED.2017.2654262.

[17] M. Wang, Y. Lv, Z. Wen, H. Zhou, P. Cui, and Z. Lin, "Monte Carlo investigation of high-field electron transport properties in AlGaN/GaN HFETs," *IEEE Electron Device Lett.*, vol. 43, no. 12, pp. 2041–2044, Dec. 2022, doi: 10.1109/LED.2022.3217127.

[18] Q. Hao, H. Zhao, and Y. Xiao, "A hybrid simulation technique for electrothermal studies of two-dimensional GaN-on-SiC high electron mobility transistors," *J. Appl. Phys.*, vol. 121, no. 20, May 2017, Art. no. 204501, doi: 10.1063/1.4983761.

[19] Y.-R. Wu, M. Singh, and J. Singh, "Device scaling physics and channel velocities in AlGaN/GaN HFETs: Velocities and effective gate length," *IEEE Trans. Electron Devices*, vol. 53, no. 4, pp. 588–593, Apr. 2006, doi: 10.1109/TED.2006.870571.

[20] F. Schwierz, "An electron mobility model for Wurtzite GaN," *Solid-State Electron.*, vol. 49, no. 6, pp. 889–895, Jun. 2005, doi: 10.1016/j.sse.2005.03.006.

[21] M. Yang, Z. Lin, J. Zhao, P. Cui, C. Fu, Y. Lv, and Z. Feng, "Effect of polarization Coulomb field scattering on parasitic source access resistance and extrinsic transconductance in AlGaN/GaN heterostructure FETs," *IEEE Trans. Electron Devices*, vol. 63, no. 4, pp. 1471–1477, Apr. 2016, doi: 10.1109/TED.2016.2532919.

[22] P. Cui, Y. Lv, Z. Lin, C. Fu, and Y. Liu, "Effect of polarization Coulomb field scattering on device linearity in AlGaN/GaN heterostructure field-effect transistors," *J. Appl. Phys.*, vol. 122, no. 12, Sep. 2017, Art. no. 124508, doi: 10.1063/1.5005518.

[23] M. Zhang, X.-H. Ma, L. Yang, M. Mi, B. Hou, Y. He, S. Wu, Y. Lu, H.-S. Zhang, Q. Zhu, J. Yin, J. Wu, L.-A. Yang, and Y. Hao, "Influence of fin configuration on the characteristics of AlGaN/GaN fin-HEMTs," *IEEE Trans. Electron Devices*, vol. 65, no. 5, pp. 1745–1752, May 2018, doi: 10.1109/TED.2018.2819178.

[24] M. Yang, Z. Gao, X. Su, Y. Wang, Y. Han, X. Tang, B. Li, J. He, J. Liu, R. Wang, X. Liu, F. Mei, L. Wang, L. Zhou, W. Song, Y. Liu, F. Wan, Z. Cui, and B. Liu, "Study of drain access resistance in saturation region of AlGaN/GaN heterostructure field-effect transistors," *IEEE Trans. Electron Devices*, vol. 69, no. 5, pp. 2293–2298, May 2022, doi: 10.1109/TED.2022.3159283.
[25] X. Cheng, M. Li, and Y. Wang, "An analytical model for current–voltage characteristics of AlGaN/GaN HEMTs in presence of self-heating effect," *Solid-State Electron.*, vol. 54, no. 1, pp. 42–47, Jan. 2010, doi: 10.1016/j.sse.2009.09.026.

MINGYAN WANG received the B.S. degree in microelectronics from Tongji University, Shanghai, China, in 2017. He is currently pursuing the Ph.D. degree with the School of Integrated Circuits, Shandong University, Jinan, China. His current research interest includes GaN-based HFETs.

YUANJIE LV received the Ph.D. degree in microelectronics from Shandong University, China, in 2018. He is currently a Senior Engineer with the National Key Laboratory of Application Specific Integrated Circuit, Hebei Semiconductor Research Institute, Shijiazhuang, China.

HENG ZHOU received the B.S. degree in microelectronics from Shandong University, Weihai, China, in 2020, where he is currently pursuing the Ph.D. degree with the School of Integrated Circuits. His current research interest includes GaN-based HFETs.

PENG CUI received the Ph.D. degree in microelectronics from Shandong University, China, in 2018. He is currently a Professor with the Institute of Novel Semiconductor, Shandong University, Jinan, China. His current research interest includes GaN-based HFETs.

ZHAOJUN LIN received the Ph.D. degree from the Institute of Semiconductors, Chinese Academy of Sciences, Beijing, China, in 1997. From 1999 to 2003, he has been with McMaster University, Hamilton, ON, Canada; Northwestern University, Evanston, IL, USA; and Ohio State University, Columbus, OH, USA. He is currently a Professor with the School of Microelectronics, Shandong University, Jinan, China. His research interest includes electronic device design and modeling.